UNIVERSITYOF BIRMINGHAM

Cutting resistance of metal-ceramic interpenetrating composites

Liu, Jing; Wu, Jinyu; Binner, Jon

[Link to publication on Research at Birmingham portal](#)

Author's Accepted Manuscript

Cutting Resistance of Metal-Ceramic Interpenetrating Composites

Jing. Liu, Jinyu Wu, Jon Binner

Cite this article as: Jing. Liu, Jinyu Wu and Jon Binner, Cutting Resistance of Metal-Ceramic Interpenetrating Composites, *Ceramics International*, http://dx.doi.org/10.1016/j.ceramint.2016.11.124

www.elsevier.com/locate/ceri

Cutting Resistance of Metal-Ceramic Interpenetrating Composites

Jing Liu*, Jinyu Wu[#], Jon Binner[¶]

* School of Materials Science & Engineering, Shanghai Jiao Tong University, 800 Dongchuan Road, Shanghai, 200240, PR China
[#] Siemens AG, St.-Martin-Str. 76, 81541, Munich, Germany
[¶] School of Metallurgy & Materials, University of Birmingham, Birmingham, B15 2TT, UK

Abstract

Metal-ceramic interpenetrating composites (IPCs) can be successfully manufactured by the pressureless infiltration of ceramic foams with molten metals. The resulting IPCs, in which both phases are three dimensionally continuous, have many potential applications, including wear and ballistic resistance amongst other uses. As these materials are extremely difficult to cut or machine, one potential application is for cut-resistant security materials. This project investigated their cutting resistance with a view to understanding the underpinning mechanisms.

The composites were produced by infiltrating Al-10wt% Mg alloy into gel-cast spinel and mullite foams of different densities at atmospheric pressure. Samples were subject to cutting using a diamond slitting wheel to determine cutting rates under different conditions and the cut products, cutting tools and debris were characterised, primarily using a range of electron microscopy-based techniques. As expected, the cutting resistance was found to be largely dependent on the hardness of the IPCs, however evidence was also found of the role that is played by the continuous metallic

phase. Plastic deformation can consume energy and bridge cracks; strain hardening under the twin actions of compression and shearing can enhance the hardness and strength of the metal at the cut tips and adhesive wear is believed to be the main origin of rapid tool failure. In addition, metal-ceramic IPCs produced via pressureless infiltration show very good interfacial bonding between the phases.

Keywords: Interpenetrating composites; Cutting resistance; Pressureless infiltration.

1. Introduction

The difficulty in machining metal matrix composites (MMCs) and related materials such as 3-3 interpenetrating composites (IPCs), which have a very intimate distribution of both continuous hard ceramic and continuous ductile metal, has been widely recognised. It limits the secondary processing of these materials [1] and hence restricts their uptake in a wide range of applications, which can include thermal substrates, heat sinks and chip carriers for the electronics industry and brake discs, cylinder bores and ventral fins in the automotive/aerospace industries, amongst others [2]. The difficulty associated with machining these materials can be considered as a useful property, however, for security applications where materials with resistance to being cut are required.

In 3-3 interpenetrating composites (IPCs), both the matrix and the reinforcement are co-continuous, resulting in two interpenetrating phases [3]. Compared with traditional

MMCs, IPCs can exhibit significant advantages such as multifunctionality and macroscopically isotropic properties [4] and, very recently, it has been shown that they can also have excellent mechanical properties [5]. It is also possible to incorporate relatively high volume fractions of one phase in the other. The fabrication of such materials, however, demands the ability to control the distribution and connectivity of the two phases. This has been achieved by infiltrating molten materials, such as metals or polymers, into preforms consisting of ceramic powder beds or highly porous ceramic foams. This can be achieved via pressureless infiltration if the wetting characteristics of the two phases are controlled[6] though others have fallen back on the use of pressure [7].The approach can be used to achieve considerable variety in terms of the composition of the ceramic phase and the composition, amount and distribution of the infiltrated phase [6,8,9]. As a result, IPCs can provide superior properties, including strength, toughness, hardness, wear resistance and high strain rate properties, over either the single components or more traditionally processed MMCs of similar composition [8,10,11]. In addition, utilising shaped preforms can result in a near-net-shape manufacturing capability, which is extremely beneficial given the aforementioned difficulty in cutting or machining these materials.

Cutting resistance is not an intrinsic material property but is determined by a range of factors, including the Young's modulus, energy dissipation capacity and coefficient of friction of the workpiece material [12]. For an MMC or metal-ceramic IPC, the inherent

nature of the matrix and the reinforcement, the volume fraction and morphology of the latter and even the nature and degree of bonding between the two phases can all influence the composite's cutting resistance. Additionally, external factors such as the cutting tool material and geometry, applied load and cutting speed also affect it [12].

According to previous work on cutting MMCs [13-15], there are two fundamental difficulties: limited options in terms of cutting tools and rapid tool failure. Whilst the limitation in many cases arises mainly as a result of the high hardness of the reinforcing ceramic phase, tool failure can be attributed to a number of reasons including severe abrasive wear and formation of chips and built-up edges [16].The twin objectives of the present research were to quantify the cutting resistance of metal-ceramic IPCs produced using the pressureless infiltration of ceramic foams with molten metal and to investigate the mechanisms underpinning it.

2. Material and Methods

2.1 Processing of metal-ceramic IPCs

Gel-cast spinel ($MgAl_2O_4$) and mullite ($Al_6Si_2O_{13}$) foams(Dyson Thermal Technology Limited, Sheffield, UK)were used as the porous ceramic preforms; the general principles of their manufacture have been provided elsewhere [17]. All of the foams used had an average cell size of ~300 μm, densities ranging from 15% to 40% of theoretical and measured 5x10x35 mm. The metal used to infiltrate the foams was an Al-10 wt% Mg alloy, produced by combining commercially pure Al and a Mg-Al master

alloy, AZ81, in the appropriate quantities in the molten state. The resulting alloy ingot was cut into coupons, the size of each coupon being the same area as the ceramic foams with a thickness designed to yield the required volume to fully infiltrate them. Given the variation in porosity of the different preforms, this meant that the coupons ranged in thickness from 4– 5 mm. All the surfaces, edges and corners of each alloy coupon were ground using different grades of SiC abrasive paper, from 80 up to 1200 grit, to remove any surface defects and the inevitable oxide layer.

Each metal / ceramic foam couple was loaded into an alumina boat and positioned horizontally in the centre of a tube furnace, figure 1. Previous work had shown that it made no difference which was on top [6,9]. The couple was heated in flowing argon at 5 cm^3min^{-1} to a process temperature of 915°C when flowing nitrogen at 20 cm^3min^{-1} was substituted for the argon. This changed the wetting characteristics between the molten metal and ceramic foam, allowing the former to penetrate spontaneously through the latter's pores. A detailed study of the wetting process has been published elsewhere [8]. Once infiltration was complete, as observed through a window in the end of the tube furnace, argon was once again fed through as the resulting interpenetrating composite was cooled. Density of the samples was determined following ASTM C20-00[18]. The final products' densities were >99% of theoretical and any porosity was disconnected.

2.2 Quantification of cutting resistance

The infiltrated Al-10Mg/spinel IPCs and Al-10Mg/mullite IPCs, together with samples of the Al-10Mg alloy and dense mullite for comparison, were ground and polished so that all had the same surface roughness of ~20 μm RA. To determine the cutting resistance, each sample was cut without lubricants in two different ways using a low speed, 500 rpm, circular saw with a 100 mm diameter blade consisting of a standard copper disc with fine diamonds inserted around the edge. The first cut lasted for exactly 30 s, after which the depth of the cut was measured precisely, in-situ, using a vernier calliper. This was followed by 5-10 minutes of further cutting during which time the remaining uncut depth was measured at 1 minute intervals, again without taking the sample out of its holder on the cutting machine. Cutting was terminated when there was <1 mm of residual material holding the two halves of the sample together. Before and after the two cuts, the blade was cleaned of debris via cutting a 20% dense mullite foam for 10 minutes. Throughout the cutting processes, falling debris was collected for characterisation. The cutting rate of each sample was calculated as:

$$\text{Cutting rate} = \frac{\sum_{i=1}^{n}(D_i - D_{i+1})}{n}$$

where D_i is the remaining uncut depth after each 1-minute-interval's cutting, and n is the total number of times the sample was cut.

Field emission gun scanning electron microscopy, FEGSEM (LEO 1530VP, Carl Zeiss SMT, Oberkochen, Germany) was used to study the microstructures of the cut faces of the samples, the tip of each cut, figure 2a, and the debris created. To further characterise the microstructures at and beneath the cut tip surface, to enable an

understanding of the cutting mechanism to be developed, a layer of platinum was deposited on some of the samples and a dual-beam focused ion beam scanning electron microscope, DBFIB-SEM (Nova 600 Nanolab, FEI Company, Hillsboro OR, USA) used to obtain cross-sections, Figure 2b, for subsequent imaging and EDS mapping.The cutting edges of the diamond blades were also examined; an infinite focus microscope, IFM (Alicona UK Ltd., Kent, UK) was used to determine their topography in the form of a 3-D height/roughness map. The morphology of the diamonds was investigated for both new and worn blades using scanning electron microscopy, SEM (Stereoscan 360, Cambridge Instruments/Carl Zeiss SMT, Cambridge, UK). For the worn blade, images were taken before and after thorough cleaning with acetone. All of the SEM images were taken with an accelerating voltage of 10 kV and an emission current of 20 mA.The duration of EDS was 40 seconds per spectrum for spot scans and 30 minutes per image for mapping, respectively. The FIB micrographs were taken with an accelerating voltage of 30 kV and an emission current of 30 pA.

3. Results and Discussion

3.1 Cutting resistance of ceramic foam reinforced IPCs

The results of the cutting tests performed are shown in figure 3; obviously the lower the cutting rate, the higher the cutting resistance. As expected, the cutting resistance of either kind of IPC increases with increasing foam density, i.e. higher ceramic content leads to higher cutting resistance. The same result has been observed for

tool wear during the cutting of MMCs [19,20]. According to Ozben et al. [20], at every

cutting speed investigated an Al-MMC containing15% SiC particles led to nearly 1.5

times higher tool wear than for a similar MMC containing just 5% SiC particles.

Similarly, the cutting resistance of the spinel-based IPCs was better than that of the

mullite-based IPCs; the cutting rate of the 20% spinel IPC was only half that of the 20%

mullite IPC. This difference will have been due to the higher hardness of spinel

compared to mullite, figure 4.Althoughit has been well documented that

metal-ceramic composites are difficult to machine due to the high hardness of the

ceramic phase, figure 4 also reveals that hardness is not the only factor. Whilst the 15%

spinel IPC had similar hardness and cutting rate to the 30% mullite IPC, the 20%

spinel IPC was almost as hard as the 40% mullite IPC, but offered a significantly

better cutting resistance. In addition, the 20% mullite IPC exhibited a similar cutting

rate to the unreinforced, and hence much softer, Al-10Mg alloy. Consequently, it is

believed that hardness is not the only contributor to the cutting resistance of

metal-ceramic IPCs; the metal phase is also likely to play a role. The effect of the

condition of the cutting blade is believed to be contained with the error bars for each

result obtained.

3.2 Microstructure characterisation

Considering the cutting process caused by the low speed circular saw, there will have

been two forces acting on each sample, viz. a vertical compressive force at the cut tip

generated by the downward pressure on the sample by the specimen holder pushing

it onto the blade and a simultaneous horizontal shear force arising from the sliding friction between the two sides of the cut sample and the blade.SEM micrographs of the cut tips for the Al-10Mg/15% spinel IPC samples after 0.5 and 5 minutes of cutting are shown in figure 5.Evidence of the two forces at work during cutting, in the form of both 'smearing' and brittle fracture of the metal phase, may be observed in figure 5(b).Severe brittle fracture of a hardened metal phase was also found by Ding et al. [21] at ridges formed in a SiC particle reinforced Al-MMC after cutting at 50 mmin^{-1}, with coolant, using a polycrystalline boron nitride (PCBN) cutting tool. Plastic deformation of the metal phase can also be found at the cut tip after longer cutting times, figure5(c)& (d). The latter can help to absorb energy and improve strength when MMCs are damaged [22].

Since the ceramic phase was rarely observed at the cut tips of any of the IPCs, the 30 min cut tip for the 15% spinel-based IPC was cross-sectioned via DBFIB and the resultant microstructure is shown in figure 6. The ceramic phase appears brighter in the secondary electron image, figure 6(a), but darker in the backscattered electron micrograph, figure 6(b). A~1 µm thick layer of metal can be observed spread across the surface in figure 6(b), just below the platinum layer deposited prior to FIBing. It is much more difficult to observe it in figure 6(a), though presumably it is also present. It is assumed that this layer was caused by the smearing of the metal phase from within the composite, although it might also have been generated by secondary adhesion of the metal debris that had originally adhered to the blade tip. Ding et al. [21] favoured

the latter explanation after cutting SiC particle reinforced Al-MMC at 400 mmin^{-1} using a PCBN tool without coolant arguing that a layer of work material had adhered to the machined surface. Their SEM micrograph revealed metallic plateau suggesting the metal debris was sheared and then deformed. In the current work, however, the cutting conditions will have been considerably less demanding.

A crack can be clearly observed in figure 6; it is assumed that it was formed by the compressive forces present. As shown by the EDS maps for Al (indicating the location of the metal phase) and O (the ceramic phase) in figures 6(c) and (d), respectively, the crack tended to propagate along the ceramic grain boundaries and was bridged by the ductile metal phase. A second, smaller crack was observed beneath the surface metal layer, figure 7. This smoother crack looks as if it might indicate brittle fracture along a grain boundary in the (probably strain hardened) metal phase. According to previous microstructural characterisation of similar IPC samples , micropores in the metal can act as preferential cracking sites [11,23].

Amongst all of the IPC cut tips and cut sections investigated, ceramic-metal debonding was never observed indicating good interfacial bonding between the two phases. This was supported by the analysis of the debris, e.g. figure 8 from the cutting of a 20% spinel IPC sample, which again included both the ceramic and metal phases in each piece of debris.

3.3 The cutting tool

The wear of the blade consisted primarily of the pull out of the diamonds, figure 9 (and some wear of the copper substrate). The extent of the damage can be seen from the infinite focus microscope, IFM, maps of new and used blades, figure 10. It is believed that the diamonds were pulled out mainly by the adhesion of the metal phase during cutting; figure 11 shows the diamond-studded edge of (a) a new blade and (b) a blade just after cutting, which shows a layer of ductile metal largely covering the diamonds. The metal layer can clearly be removed by cleaning, figure 11(c). A more detailed observation of the old blade just after cutting, showing severe debris built-up, is shown in figures 11(d) and (e). This 'built-up edge' (BUE) phenomenon has been reported several times in the literature for the cutting of MMCs [24-26]. Manna et al. [26] defined BUE as the repeated addition of debris to the blade edge under conditions of high friction, pressure and temperature. It is probable that as the adhering debris is removed during cleaning to expose the diamonds again, some of the latter are plucked out. Andrewes et al. [27] proposed the idea that in the initial stage of cutting Al/SiC composites, the flank wear of the polycrystalline diamond (PCD) tooling was mainly abrasive wear by the ceramic phase, but, as cutting progressed, both this and adhesive wear by the removal of the adhered metal phase occurred. Similar results were seen in the current work, as illustrated by figure 12, which shows the occurrence of cracking, chipping, surface spalling and diamond pullout at a used blade edge.

3.4 Understanding cutting resistance by interpenetrating composites

Whilst it is well-known that the high hardness of the continuous ceramic phase in ceramic reinforced IPCs is the primary contributing factor to their excellent cutting resistance, it is believed that the metal phase also contributes, figure 13. When a metal-ceramic IPC is compressed and sheared, some of the metal phase in the ceramic cells is extruded and smeared across the surface, forming, it is believed, a strain hardened thin metallic layer in a manner similar to the drawing of a metal [28]. As a consequence, it takes more stress to deform the metal phase after continuous cutting for a period of time. The significant effect of dislocation density on yield stress is shown in the equation below [28]:

$$\sigma_0 = \sigma_i + \frac{1}{2}Gb\rho^{1/2}$$

where σ_0 is the yield stress, σ_i is the initial strength, G is the shear modulus of the material, b is the burgers vector and ρ is the dislocation density. As a result, most mechanical properties, including strength, hardness and wear performance, are enhanced anisotropically [28], but toughness is reduced, resulting in brittle fracture of the strain hardened metal at ridges under shearing. In addition, metal-ceramic IPCs produced via pressureless infiltration show very good interfacial bonding between the phases, whilst cracks in traditional MMCs usually initiate from debonding between ceramic particles and the metal matrix during cutting [26].

4. Conclusions

The cutting resistance of Al-alloy/spinel and Al-alloy/mullite IPCs has been assessed and the results indicate that higher hardness, from either the incorporation of a higher density ceramic foam or the use of a harder ceramic material, generally results in superior cutting resistance as expected. However, the evidence also suggests that the metal phase can make a significant contribution. Plastic deformation can consume energy and bridge cracks; strain hardening under the twin actions of compression and shearing can enhance the hardness and strength of the metal at the cut tips and adhesive wear is believed to be the main origin of rapid tool failure. In addition, metal-ceramic IPCs produced via pressureless infiltration show very good interfacial bonding between the phases.

Acknowledgements

References

[1] A. Manna, B. Bhattacharyya, A Study on Different Tooling Systems during Machining of Al/SiC-MMC, J. Mater. Process. Tech. 123 (2002) 476-482.

[2] A. Evans, C. S. Marchi, A. Mortensen, Metal Matrix Composites in Industry: an Introduction and a Survey, Kluwer Academic, London, 2003.

[3] R. E. Newnham, D. P. Skinner, L. E. Cross, Connectivity and Piezoelectric-pyroelectric Composites, Mater. Res. Bull. 13 (1978) 525-536.

[4] D. R. Clarke, Interpenetrating Phase Composites, J. Am. Ceram. Soc. 75(4) (1992) 739-759.

[5] L. Hu, M. O'Neil, V. Erturun, R. Benitez, G. Proust, I. Karaman, M. Radovic, High-Performance Metal/Carbide Composites with Far-From-Equilibrium Compositions and Controlled Microstructures, Sci. Rep. 6 (2016) 35523.

[6] J. G. P. Binner, H. Chang, R. Higginson, Processing of Ceramic-metal Interpenetrating Composites, J. Eur. Ceram. Soc. 29 (5) (2008) 837-842.

[7] L. Hu, A. Kothalkar, M. O'Neil, I. Karaman, M. Radovic, Current-Activated, Pressure-Assisted Infiltration: A Novel, Versatile Route for Producing Interpenetrating Ceramic-Metal Composites, Mater. Res. Lett. 2 (2014) 124-130.

[8] J. Liu, J. Binner, R. Higginson, Z. Zhou, Interfacial reactions and wetting in Al-Mg/oxide ceramic interpenetrating composites made by a pressureless infiltration technique, Compos. Sci. Technol. 72 (2012) 886-893.

[9] J. Liu, J.G.P. Binner, R. Higginson, Dry sliding wear behaviour of co-continuous ceramic foam aluminium interpenetrating composites produced by pressureless infiltration, Wear 276-277 (2012) 94-104.

[10] H. Chang, J. G. P. Binner, R. Higginson, Dry Sliding Wear Behaviour of Al(Mg)/Al$_2$O$_3$ Interpenetrating Composites Produced by a Pressureless Infiltration Technique, Wear 268 (2010) 166–171.

[11] H. Chang, J. G. P. Binner, R. Higginson, High Strain Rate Characteristics of 3-3

Metal–Ceramic Interpenetrating Composites, Mat. Sci. Eng. A 528 (2011) 2239–2245.

[12] B. N. Vu Thi, T. Vu-Khanh, J. Lara, Mechanics and Mechanism of Cut Resistance of Protective Materials, Theor. Appl. Fract. Mec. 52 (2009) 7–13.

[13] L. Cronjager, D. Meister, Machining of Fibre and Particle-reinforced Aluminium, CIRP Ann. – Manuf. Techn. 41(1) (1992) 63-66.

[14] J. P. Davim, A. M. Baptista, Relationship between Cutting Force and PCD Cutting Tool Wear in Machining Silicon Carbide Reinforced Aluminium, J. Mater. Process. Tech. 103 (2000) 417–423.

[15] J. P. Davim, A. M. Baptista, Cutting Force, Tool Wear and Surface Finish in Drilling Metal Matrix Composites, P. I. Mech. Eng. E-J. Pro. 215 (2001) 177–183.

[16] J. M. Monaghan, P. O'Reilly, The Drilling of an Al/SiC Metal Matrix Composites, J. Mater. Process. Tech. 33 (1992) 469-480.

[17] P. Sepulveda, J. G. P. Binner, Processing of Cellular Ceramics by Foaming and In-situ Polymerisation of Organic Monomers, J. .Eur. Ceram. Soc. 19 (1999) 2059-2066.

[18] ASTM, ASTM International, C20-00, 2010.

[19] Q. Yamming, Z. Zehua, Tool Wear and its Mechanism for Cutting SiC Particle-reinforced Aluminium Matrix Composite, J. Mater. Process. Tech. 100 (2000) 194-199.

[20] T. Ozben, E.Kilickap, O. Cakır, Investigation of Mechanical and Machinability Properties of SiC Particle Reinforced Al-MMC, J. Mater. Process. Tech. 198 (2008) 220–225.

[21] X. Ding, W. Y. H. Liewb, X. D. Liu, Evaluation of Machining Performance of MMC with PCBN and PCD Tools, Wear 259 (2005) 1225–1234.

[22] S.R. Boddapati, J. Rödel, V. Jayaram, Crack Growth Resistance (R-curve) Behaviour and Thermo-Physical Properties of Al_2O_3 Particle-Reinforced AlN/Al Matrix Composites, Compos. Part A – Appl. S. 38 (2007) 1038-1050.

[23] D.A.H. Hanaor, L. Hu, W.H. Kan, G. Proust, M. Foley, I. Karaman, M. Radovic, Compressive performance and crack propagation in Al alloy/Ti_2AlC composites, Mater. Sci. Eng. A 672 (2016) 247-256.

[24] M. El-Gallab, M. Sklad, Machining of Al/SiC Particulate Metal Matrix Composites. Part I: Tool Performance, J. Mater. Process. Tech. 83 (1998) 151–158.

[25] M. El-Gallab, M. Sklad. Machining of Al/SiC Particulate Metal Matrix Composites. Part II: Workpiece Surface Integrity, J. Mater. Process. Tech. 83 (1998) 277–285.

[26] A. Manna, B. Bhattacharyya, A Study on Machinability of Al/SiC-MMC, J. Mater. Process. Tech. 140 (2003) 711–716.

[27] C.J. E. Andrewes, H. Y. Feng, W. M. Lau, Machining of an Aluminum/SiC Composite Using Diamond Inserts, J. Mater. Process. Tech. 102 (2000) 25–29.

[28] J. H. Westbrook, R. L. Fleischer, Intermetallic Compounds - Principles and Practice: Progress, Volume 3, John Wiley & Sons, 2002.

Figure Captions

Figure 1: Schematic of (a) the furnace arrangement and (b) the arrangement of the metal/ceramic couples inside the tube furnace for the production of metal-ceramic interpenetrating composites (IPCs).

Figure 2: Schematic diagrams illustrating a) how the tip of each cut was analysed by SEM (the cut surfaces were also examined) and b) the location of the cross sections removed by DBFIB for imaging and EDS analysis, marked by the white line.

Figure 3: Cutting rates of all samples tested

Figure 4: Relationship between hardness and cutting rate

Figure 5: SEM micrographs of cut tips in the Al-10Mg/15% spinel-based IPC sample after (a) and (b) 0.5 minute's cutting; (c) and (d) 5 minutes' cutting.

Figure 6: (a) Secondary electron and(b)back scattered SEM micrographs of a DBFIB cross section taken from beneath a 30 min cut tip in the 15% spinel IPC and corresponding EDS maps for(c) Al and (d) O. The crack shows evidence of metal bridging.

Figure 7: A backscattered SEM micrograph of a different crack found below the crack tip in a 15% spinel IPC sample after 30 min of cutting.

Figure 8: (a) An SEM photograph of cut debris from a 20% spinel IPC and (b) EDS analysis of two locations in the same flake showing the presence and absence of the O peak, which is indicative of the presence of the ceramic phase.
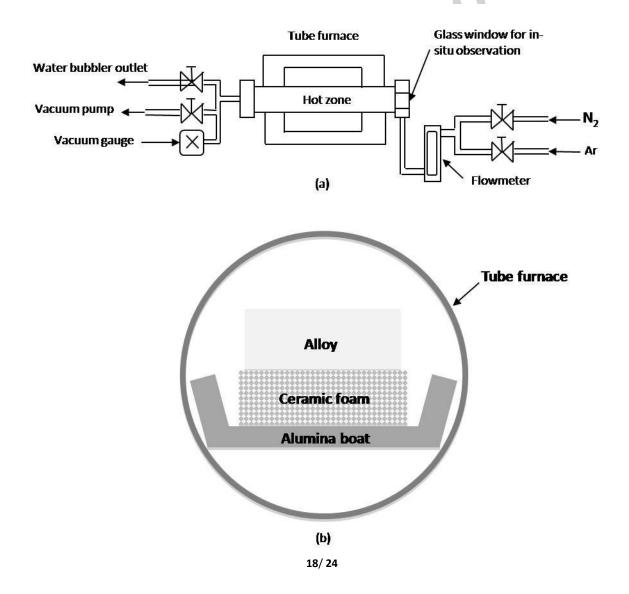
Figure 9: SEM images of (a) a diamond in the edge of the copper blade and (b) the void left behind after a diamond had been pulled-out of a blade after use.
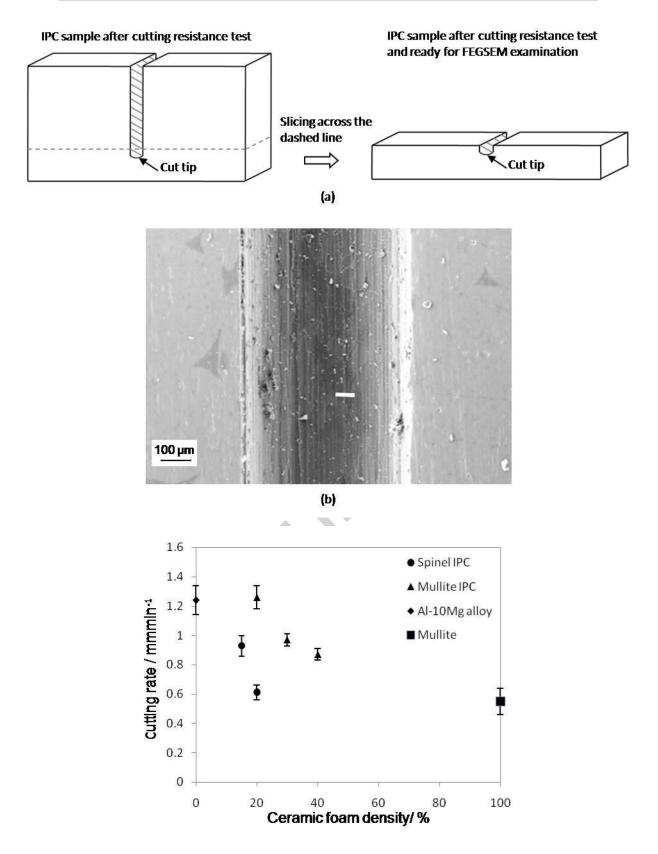
Figure 10: Infinite focus microscope, IFM, maps of the edges of (a) a new diamond cutting blade and (b) an old blade.
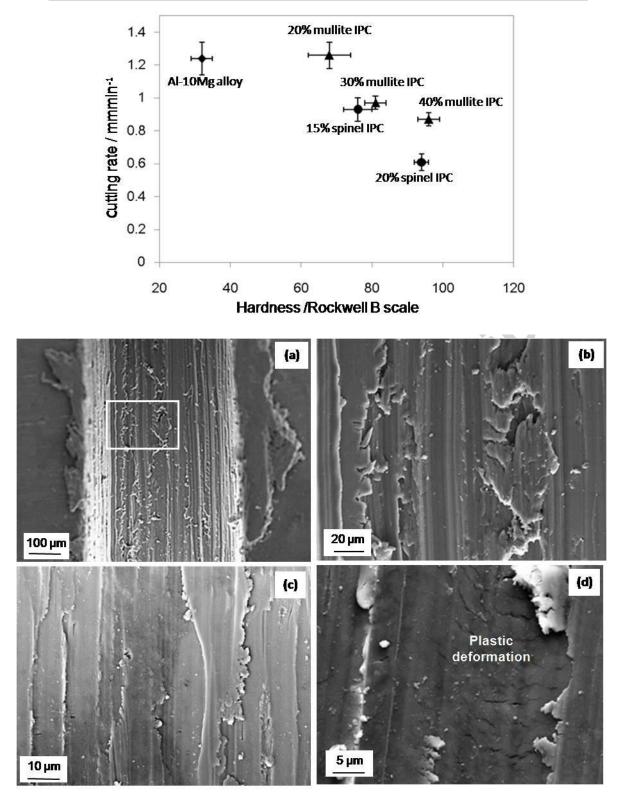
Figure 11: SEM micrographs of the diamond-studded edge of (a) a new blade, (b)a used blade just after cutting, (c) the same blade after cleaning. (d) and (e) show the debris build up during cutting at higher magnifications.
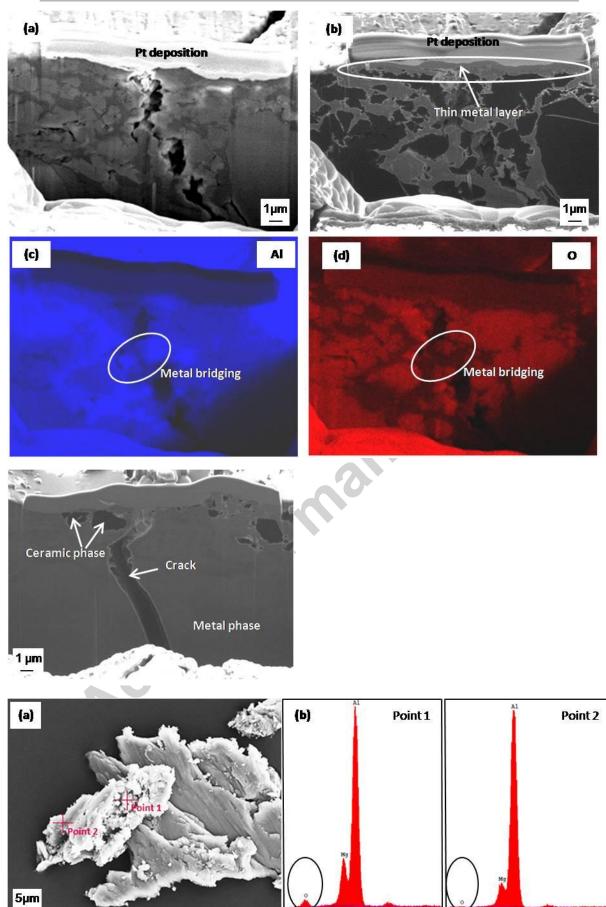
Figure 12: SEM photographs of (a) cracking,(b) chipping,(c)surface spalling and (d) diamond pullout at a used blade edge.

Figure 13: Proposed schematic of a metal-ceramic IPC under the twin actions of compression and shearing during cutting.
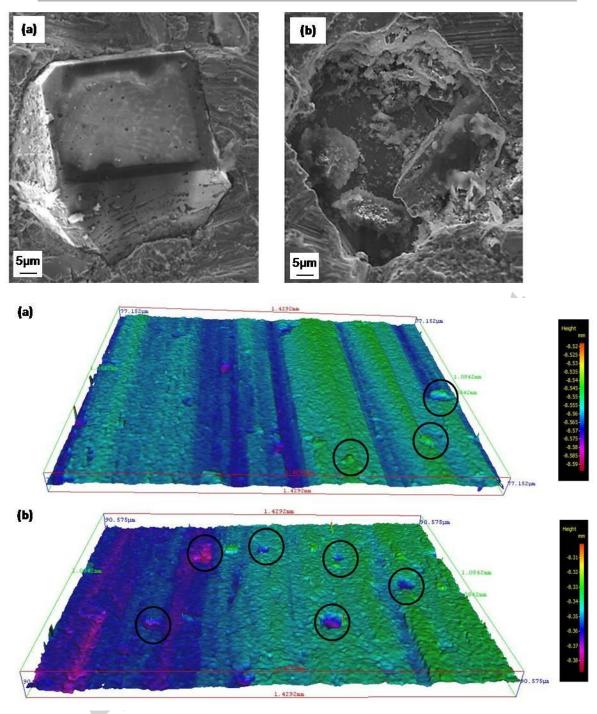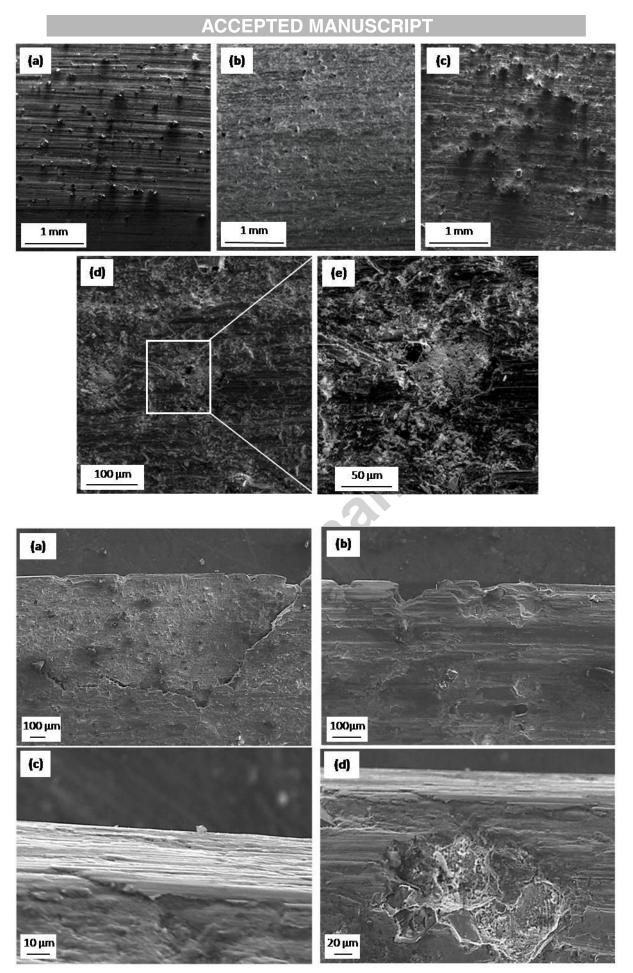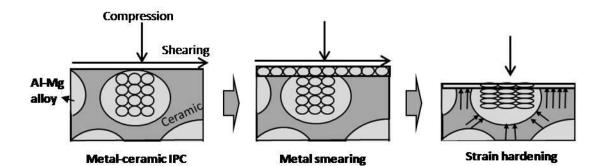

(a)

(b)

IPC sample after cutting resistance test

IPC sample after cutting resistance test and ready for FEGSEM examination

Slicing across the dashed line

Cut tip

Cut tip

(a)

100 μm

(b)

- Spinel IPC
- Mullite IPC
- Al-10Mg alloy
- Mullite